Solar Energy 188 (2019) 1178–1188

Contents lists available at ScienceDirect

Solar Energy

journal homepage: www.elsevier.com/locate/solener

Efficient and cost-effective dye-sensitized solar cells using MWCNT-TiO_2 nanocomposite as photoanode and MWCNT as Pt-free counter electrode

M. Younas[a], M.A. Gondal[a,b,*], M.A. Dastageer[a], K. Harrabi[a]

[a] Laser Research Group, Department of Physics, Center of Research Excellence in Nanotechnology (CENT), King Fahd University of Petroleum and Minerals (KFUPM), P.O. Box 5047, Dhahran 31261, Saudi Arabia

[b] K.A.CARE Energy Research & Innovation Center at King Fahd University of Petroleum and Minerals, P.O. Box 5047, Dhahran 31261, Saudi Arabia

ARTICLE INFO

Keywords:
Multiwall carbon nanotubes (MWCNT)
DSSC
Photovoltaic
Electrochemical
Efficiency
Renewable energy

ABSTRACT

In the present study, a new cost-effective and efficient configuration [*n*-MWCNT-TiO_2/N3/MWCNT] of dye-sensitized solar cell (DSSC) is proposed and fabricated, where *n*-MWCNT-TiO_2 is the nano composite of multiwall carbon nanotube (MWCNT), and titanium dioxide (TiO_2) in different mass proportions, sensitized by N3 dye used as a photo anode, and MWCNT is the material for the counter electrode. In the [*n*-MWCNT-TiO_2/N3/MWCNT] configuration, the photo anode with four mass proportions (n = 0.03%, 0.06%, 0.09% and 0.12%) were used as a design variant, and it was found that the photovoltaic efficiency as high as 7.15% was achieved when the nano composite of 0.06%-MWCNT-TiO_2 was applied as a photoanode in the proposed DSSC configuration. Besides achieving a 13% photovoltaic efficiency enhancement compared to the ubiquitous [TiO_2/N3/Pt] DSSC configuration, the replacement of Pt with inexpensive MWCNT in the [*n*-MWCNT-TiO_2/N3/MWCNT] DSSC ensures the cost effectiveness of the proposed configuration. The morphological and optical characterization of the *n*-MWCNT-TiO_2 photoanode (nanocomposite) films, the stability and catalytic activity of MWCNT counter electrode, UV–VIS absorption spectroscopy, current-voltage characteristics, incident photon to electron conversion efficiency and the electrochemical impedance spectroscopy of the fabricated DSSCs were performed in order to elucidate the improved performance of the [*n*-MWCNT-TiO_2/N3/MWCNT] configuration. Based on these characterization studies, it was found that the observed enhancement of light absorbance in the visible spectral region, the improved electron transportation, decreased recombination of electrons with oxidized dye and redox mediator, better catalytic activity of MWCNT counter electrode are the key contributory factors for the increased photovoltaic efficiency of the [*n*-MWCNT-TiO_2/N3/MWCNT] DSSC configuration.

1. Introduction

Ever increasing global need, over dependency on the fast depleting fossil fuels and consequent environmental repercussions due to CO_2 emission instigated the quest for renewable energy sources particularly from abundant solar energy through photovoltaic process (Grätzel, 2009; Li et al., 2006; Mehmood et al., 2014). Photovoltaic technology has been going through three generations of research and development, mainly focusing on novel materials that could replace ubiquitous, yet expensive silicon based first generation solar cells, which achieved an efficiency of 20% (Dale, 2013). The second generation solar cells are developed from the thin films of semiconducting materials such as cadmium telluride (CdTe), amorphous silicon, or copper indium gallium selenide (CIGS) and the major constraint in the maturity of the second generation solar cell is the use of rare elements that restrict large scale production (Jacoby, 2016). Dye-sensitized solar cells (DSSC) are the third generation low-cost multi junction solar cells pioneered by Brain O'Regan and M Grätzel in 1991, in which an organic dye is excited by solar radiation, the photo generated electrons are injected to the conduction band of mesoporous semiconductor, the oxidized dye is regenerated by iodide/triiodide redox mediator and this circuit is completed by the reduction of redox couple by the incoming electron at a platinum counter electrode (Iqbal and Khan, 2018; O'Regan and Grätzel, 1991; Zulkifili et al., 2015).

The output voltage of DSSC depends on the energy difference between the quasi Fermi level of the semiconductor and the redox potential of the redox mediator under illumination and the photo-generated current depends on the absorption coefficient of the dye and the charge transportation characteristics of the dye stained semiconductor as well as the dye/TiO_2 interface. Having more dye stained mesoporous

* Corresponding author at: Laser Research Group, Department of Physics, Center of Research Excellence in Nanotechnology (CENT), King Fahd University of Petroleum and Minerals (KFUPM), P.O. Box 5047, Dhahran 31261, Saudi Arabia.
E-mail address: magondal@kfupm.edu.sa (M.A. Gondal).

https://doi.org/10.1016/j.solener.2019.07.009
Received 23 January 2019; Received in revised form 14 June 2019; Accepted 2 July 2019

semiconductor in the photoanode (larger surface area) leads to the creation of more photo generated electrons and consequently it leads to the enhancement in the efficiency of DSSC, however, with the increase of interfacial area between the photoanode and the electrolyte, the probability of recombination of conduction electrons of the semiconductor (or in any trap state) and the diffused cations of the redox couple increases, which contributes negatively to the cell efficiency. So in order to get good efficiency of a fabricated dye-sensitized solar cell, the dye in the photoanode should have high visible light absorption coefficient and the excited energy levels of the dye and the level of conduction band of the semiconductor should be favorable for a good electron transfer from the excited dye to the conduction band of the semiconducting material, compatible redox potential that enables effective regeneration of dye and the faster catalytic activity of the counter electrode in reducing the oxidized electrolyte (Hagfeldt et al., 2010; Younas et al., 2018b).

Unlike in the p-n junction photovoltaics, where the separation of the charges is mediated by the induced field in the junction, in DSSC the charge separation is realized by different competing kinetic and diffusion processes. The rate of injection of photo generated electron from the excited dye to the conduction band of the semiconductor should be higher than that of the relaxation time of the dye. In this process effective charge separation is achieved in which the electron moved from the excited dye to the conduction band of the semiconductor and the hole remained behind in the oxidized dye molecule. Then the oxidized dye molecules are reduced by the redox mediator. This process is called dye regeneration and this process should be faster than the process in which the electrons in the semiconductor are recombined with the oxidized dye and the redox mediator called as dark current or charge recombination. Also the time taken for the electron to diffuse through the semiconductor should be faster than recombination time and the diffusion length of the conduction electrons should be more than the thickness of the semiconductor coating for the efficient charge extraction (Grätzel, 2003; Hardin et al., 2012). The main advantages of DSSC over silicon based solar cell are that they are low cost design, good performance under low light condition, and do not require high crystallographic perfection in the material. In order to utilize these positive features of DSSC and to improve its photovoltaic efficiency and to outdo the performance of silicon based solar cells, research works have been directed towards the areas like, improving spectral region of the dye absorption, replacing weather incompatible electrolyte with all solid state materials, and replacing expensive platinum counter electrode with less expensive materials. The photocurrent in the conventional silicon based solar cell is due to the diffusion of electrons and holes in the space charge region and hence, the performance of silicon based solar cells is quite sensitive to the crystallographic defects in silicon, and therefore expensive defect free silicon material is required to enhance the efficiency of solar cells. On the other hand, in DSSC photons absorbed by the organic dye gives rise to electrons, which are transferred into the conduction band of semiconductors and hence, the crystallographic defects in the material is not that detrimental for the generation of photocurrent. Therefore, in spite of the better efficiency of silicon based solar cells, advantage of DSSC is that it can be made of low-cost materials and can be constructed without any advanced process technology. The Si based solar cells; the maximum achievable efficiency is intensity dependent and its performance decline in low light condition, whereas DSSC can maintain its achievable efficiency even at low light condition due to the excellent optical absorbance of the dye (Ruhle et al., 2015).

The intrinsic properties of semiconductor material and the dye used in the photoanode, redox mediator and the catalyst as counter electrode along with the thickness and structure are the key parameters that decides the interplay of different kinetic and diffusion processes leading up to the enhanced efficiency of DSSC. The light absorbance, electron injection from the dye, inhibition of recombination, electron transport is the key properties of semiconductor material in the photoanode. Many combinations semiconducting materials like ZnO, WO_3, with compatible dyes and redox couples were tried and it was established that the combination of TiO_2 with Ru based dyes and iodine electrolyte is the most suitable due to its inherent electron transport properties of TiO_2 and its compatible energy band structure with dye and redox couple, its abundance, cost effectiveness, non-toxicity and strong adsorption of dye as well as more mesoporous structure along with stability (Roy-Mayhew and Aksay, 2014; Ye et al., 2015). In spite of all these positive characteristics of TiO_2, electron transport property of TiO_2, which decides the key photocurrent in DSSC is weaker than other semiconductors like ZnO (Chandiran et al., 2014) and this deficiency of this wonderful material can be improved by synthesizing nanocomposite of TiO_2 with other suitable material and several works in the area of DSSC with composite photoanode, with improved electron transport, dye adsorption and overall increase of efficiency have been reported (Gondal et al., 2016a,b, 2015; Ilyas et al., 2016; Mehmood et al., 2018; Younas et al., 2018a). Also as mentioned above there have been many works aiming at improving the transport property of photoanode based on pure TiO_2 by doping with foreign elements and making other composites. It was reported by Tettey et al. that the presence of MWCNT in TiO_2 enhanced the material conductivity and hence it is promising for the fabrication of efficient DSSCs (Tettey et al., 2010). This motivated us to try MWCNT-TiO_2-nanocomposite as a photoanode material.

Multiwall carbon nanotubes (MWCNT) discovered by Iijima (1991) in 1991 has unique electrical and morphological characteristics, that addition of small amount of MWCNT in TiO_2 can enhance the key electron transport characteristics, when this composite is used as a semiconductor material in the photoanode of DSSC. The enhancement of electron transport in this material can be attributed to one dimensional structure and the formation of complex interpenetrating network of MWCNTs (Du et al., 2013).

The role of material of the counter electrode (CE) of DSSC is to catalyze effective reduction of oxidized electrolyte in order to win over the recombination of conduction electrons of the photo anode semiconducting material with electrolytic cations. As platinum (Pt) is well known for its chemical stability, catalytic activity and high exchange current densities, this expensive noble metal is widely used as a CE in DSSC. However, the use of platinum raises the cost of production and hence the very purpose of using DSSC in the place of silicon solar cell is not completely justified. Many groups have tried Pt- free counter electrode with carbon based and other cheap material based counter electrodes to enhance the efficiency and to reduce the cost (Lee et al., 2010; Arulraj et al., 2018; Chen and Shao, 2016; Karthick et al., 2018; Ahmed et al., 2018). These cost effective materials include carbon black, conductive polymer and carbon nanotubes as a counter electrode material (Iqbal and Khan, 2018; Mehmood et al., 2016a; Wu et al., 2017) to enhance the performance and reduce the cost of DSSCs. In this focus of improvisation of the counter electrode, MWCNT has also been tried owing to its positive attributes like high surface area and rapid electron transport (Nugent et al., 2001).

In this work, *n*-MWCNT-TiO_2 nanocomposite with four varying mass ratios of MWCNT in TiO_2 (n = 0.03%, 0.06%, 0.09 and 0.12%) were synthesized, coated on FTO and soaked in N3 dye and these dye soaked *n*-MWCNT-TiO_2 films on FTO were used as photo anodes for the fabrication of DSSC, in conjunction with iodide/triiodide redox mediator and pure MWCNT coated FTO as counter electrode. The performance evaluation of the fabricated DSSC was carried out by IV characterization, which showed the highest efficiency of 7.15% in [0.06%-MWCNT-TiO_2/N3/MWCNT] DSSC configuration, which accounts for 13% enhancement in the overall efficiency compared to the conventional [TiO_2/N3/Pt] DSSC. The improved efficiency of DSSC brought about by 0.06%-MWCNT-TiO_2 photo anode is explained in the light of the results of morphological (SEM, TEM), elemental and chemical state (XPS) and optical (absorption spectrum) of characterizations of *n*-MWCNT-TiO_2, incident photon to electron conversion efficiency (IPCE) and

electrochemical (EIS) analysis of the fabricated DSSC. The improved light absorbance in the visible spectral region, high electron recombination resistance with oxidized dye and redox mediator, improved electron transportation and better catalytic activity of MWCNT at the counter electrode are some positive attributes for the improved performance of the [0.06%-MWCNT-TiO_2/N3/MWCNT] DSSC. As for this proposed [*n*-MWCNT-TiO_2/N3/MWCNT] DSSC configuration in particular, it has not been reported in the literature to the best of our knowledge.

2. Methods and materials

2.1. Preparation of pastes for photo-anode and counter electrode (n-MWCNT -TiO_2)

Materials: FTO (SnO_2/F fluorine doped tin oxide, thickness 2.2 mm, 7 ohm/sq) conductive glass substrates, N3 dye (Ruthenium based dye), Titanium dioxide paste (Ti-Nanoxide T/SP, 14412), electrolyte Iodolyte (Z-50, 35112), were purchased from "Solaronix, Switzerland". Multiwall carbon nanotubes with outer radius 5–10 nm and length ~1–10 μm was purchased from "Chengdu Organic Chemicals Co. Ltd, China".

Preparation of photoanode: 20 mg/25 ml MWCNT suspension was prepared in ethanol and the mixture was sonicated for 12 h to get a proper dispersion of MWCNT in ethanol. For instance, in order to prepare 0.03% MWCNT-TiO_2, 38 μl of the above MWCNT suspension is added to 40 mg of TiO_2 paste and similarly for preparing 0.06%, 0.09% and 0.12% MWCNT in TiO_2, we had to add 76 μl, 114 μl, 152 μl of MWCNT suspension respectively in 40 mg of TiO_2. The prepared MWCNT/TiO_2 composite pastes with varying wt% was deposited on cleaned FTO glass substrates first by casting scotch tape (Manufacturing company: 3 M) for the desired active area and then using doctor blade method for the deposition of the prepared pastes and sequentially annealed at 150 °C for 10 min and 475 °C for next 30 min. The thickness of the prepared photoanodes was determine using SEM cross-sectional view. We found the thickness of 9 μm (on average) which has been provided in the Fig. S8.

Preparation of counter electrode: 10 mg MWCNT in 90 mg TiO_2 was mixed and a few drops of ethanol were added to the MWCNT-TiO_2 composite paste for good dispersion. The role of TiO_2 paste was like a binder which binds MWCNT together and works as an adhesive between MWCNT and FTO glass substrates. The prepared paste was deposited with the same tape casting and doctor blade method and calcined at directly 450 °C for 20 min to get the final CE for DSSC fabrication.

2.2. Fabrication of DSSCs

The photo anode substrates were soaked in the dye solution (N3 in ethanol: 0.5 mM) for 24 h. After 24 h the photoanodes were removed from dye solution and rinsed with ethanol to remove unabsorbed dye. Finally, the photoanode and the counter electrode were joined together with super glue gel (Manufacturing company: The original super glue corporation) and the electrolyte, Iodolyte Z-50 was poured between the two joined electrodes to complete the fabrication of DSSC. The optical images of as-fabricated DSSCs is provided in Fig. S7. The active area of fabricated DSSC was 0.25 cm^2.

3. Experimental results and discussions

3.1. Morphological analysis of best performing MWCNT-TiO_2 nanocomposite photo-anode

The shape, size and the composition of the semiconducting material used in the photo anode of DSSC are the key factors that profoundly influence the overall efficiency of DSSC, as these morphological characteristics of the surface of photo anode are contributory factors for the effective surface area, the nature of dye loading, the formation of trap states below the conduction band, the diffusion length of the electrons in the semiconducting layer and the number of available trajectories that electrons can pass through (Chou et al., 2007; Nakade et al., 2003). The increased surface area in smaller semiconducting particles in photo anode leads to higher dye adsorption, leading up to the generation of more number of charge carriers and consequently better photovoltaic efficiency than the DSSC having photo anode with large particle size. However, having very small particle size may lead to increased number of grain boundaries, through which electrons have to pass and the electron trapping probability is quite high (Gracia et al., 2004; Gregg et al., 2001). Moreover, the larger particles are prone to increased light scattering and hence the effective light intensity in the DSSC becomes less. Also the optimum thickness and the surface roughness of the coating on the photo anode are important factors to be considered, because larger the thickness of the coating, more is the absorbance of the dye, but at the same time the thicker coating imposes longer distance for the electrons to travel and this restricts the effective transportation of photo generated electrons to the electrode due to the increase of the charge transfer resistance. Although the thicker coating in the photo anode generate more photocurrent due to the increased building up of dye in the anode material, the light transmittance and consequent light intensity reaching the system decreases. Hence, the optimum thickness should be based on the on the nature, size and the electron transport properties of the coated anode material.

The surface morphology of the coated films of pure TiO_2 and MWCNT-TiO_2 using scanning electron microscopic (SEM) images are shown in Fig. 1a and b respectively, where the surface of TiO_2 is found to be quite porous, while in MWCNT-TiO_2 surface, MWCNT and TiO_2 particles are well dispersed. Also, the presence of a carbon peak in the EDX spectrum of MWCNT-TiO_2 in Fig. 1c, confirms the anchoring of MWCNT on TiO_2 surface. More resolved surface morphological analysis of the photo anodes was conducted by tunneling electron microscope (TEM) images shown in Fig. 2a for TiO_2 and Fig. 2b–d for MWCNT-TiO_2 with different resolutions, which gives further visual confirmation of dispersion of MWCNT in MWCNT-TiO_2 nanocomposite. The MWCNTs in photo anode are with 10–20 nm outer diameters and 1–10 μm length according to manufacturer's specification and from the TEM images, the particle size of TiO_2 is around 20 nm. It is quite clear from the TEM images in Fig. 2b and c that many TiO_2 particles anchor on the outer surface of the long tubular MWCNT and this assembly ensures the efficient electron transport through MWCNTs. With this improved electron transport due to the presence of MWCNT, there is a possibility to increase the thickness of the coating and consequently to improve the building up of dye on the anode material and thereby increasing the photocurrent without compromising the electron injection to the electrode. The HRTEM image of MWCNT in Fig. 2d shows that the spacing between adjacent MWCNT walls is around 0.346 nm. The X-ray mapping analysis in Fig. S2 was carried out to verify the uniformity of the distribution of MWCNT in TiO_2, clearly shows the uniform distribution of MWCNT in the MWCNT-TiO_2 nanocomposite anode thin films.

3.2. XPS analysis of nMWCNT-TiO_2 photo-anode

The chemical states of Titanium (Ti), Oxygen (O) and Carbon (C) atoms in the MWCNT-TiO_2 composite environment and the possible bond formation between the host and the dopant atoms were investigated using XPS. The XPS analysis of best performing sample i.e. 0.06%MWCNT-TiO_2 nanocomposite anode has been provided in Fig. 3 and the information regarding the deconvoluted peaks of this sample has been provided in Table 1. The XPS survey scan in Fig. 3a shows the presence of obvious Ti 2p, O 1s and C 1s peaks in the composite material, and in order to get the intricate details, each of the peaks in the survey scan was deconvoluted to see the nature of component peaks. In Fig. 3b, Ti 2p peak has two component peaks: Ti $2p_{3/2}$ centered at

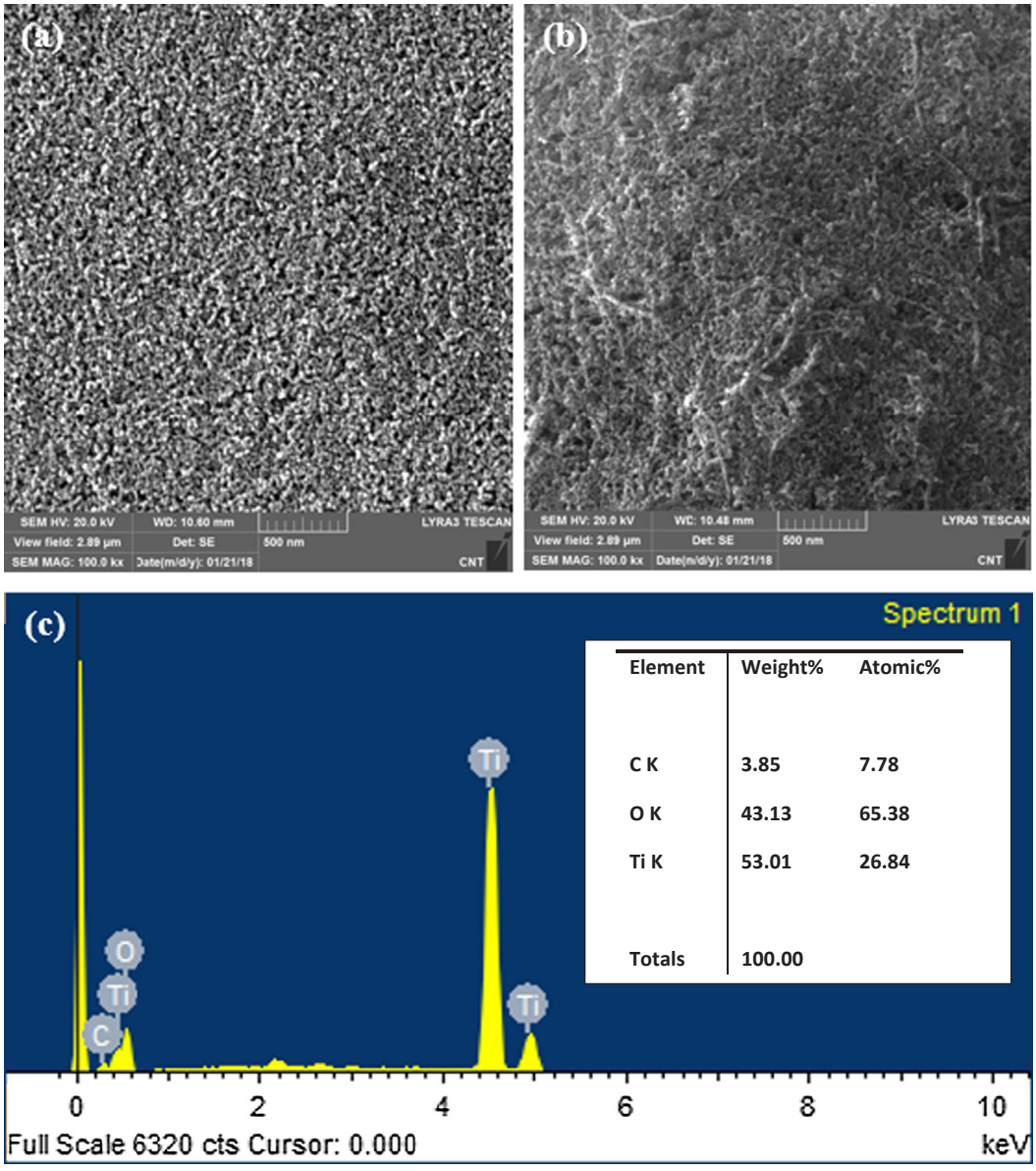

Fig. 1. SEM images of (a) pure TiO_2 (b) MWCNT-TiO_2 nanocomposite (c) EDX analysis of MWCNT-TiO_2 anode film.

459.41 eV and Ti $2p_{½}$ centered at 465.1 eV, which appear due to the spin orbit coupling, and it can be observed that these two peaks are shifted towards higher binding energies compared to the Ti 2p peaks in pure TiO_2. This shifting of Ti 2p peaks indicates that Ti in MWCNT-TiO_2 is in a different chemical state compared to Ti in pure TiO_2 and this could be ascribed to the strong interaction between TiO_2 nanoparticles and MWCNT through Ti—O—C bonding (Sanjinés et al., 1994; Sleigh et al., 1996). Also, in the deconvolution of O 1s peak in Fig. 3c, there are two component peaks centered at 531.7 eV and 530.63 eV which are attributed to the new chemical state of O atom in Ti—O and Ti—O—C bonds respectively in MWCNT-TiO_2. The intense Ti—O—C XPS peak of O 1s centered at 531.7 eV indicates a strong bonding between MWCNTs and TiO_2 in MWCNT-TiO_2 composite (Mehmood, 2017; Shuttleworth, 1980). Finally, in the deconvolution of C 1s peak, the component peaks centered at 284.65 eV, 285.81 eV, 288.65 eV and 289.23 eV are attributed to the carbon atoms in the chemical state of C—C, C—O, C═O and O—C═O respectively in MWCNTs. The formation of Ti—O—C bond in the MWCNT-TiO_2 observed from the deconvolution of Ti 2p peak is desired as it introduces a trap states in the MWCNT-TiO_2 composite. This trap state narrows down the band gap energy of MWCNT-TiO_2 composite and consequently transform the material into visible light active and makes the DSSC efficient under visible region of the solar spectrum. Also, Ti—O—C bond serves as a bridge for efficient charge transfer in the anode coating and thereby reduces the electron-hole recombination in the MWCNT-TiO_2 and increases the efficiency of the solar cell. Moreover, the anode films were prepared in the open environment which may leads to the reduction of carbon into carbon oxides which further enhance the conductivity of the photoelectrons in the anode thin films (Qiu et al., 2015). The detailed XPS analysis for all the remaining four samples i.e. *n*MWCNT-TiO_2 (n = 0%, 0.03%, 0.09% and 0.12%) was provided in Figs. S3–S6, along with the peak positions of the deconvoluted elemental peaks in Tables S1–S4. XPS of all these samples shows the presence of their respective elements as expected. The *n*MWCNT-TiO_2 thin films show the presence of both MWCNT and TiO_2 and shifting of their binding energies shows their composite formation.

3.3. XRD analysis of *n*MWCNT-TiO_2 photo-anode

The XRD analysis for all the fabricated *n*MWCNT-TiO_2

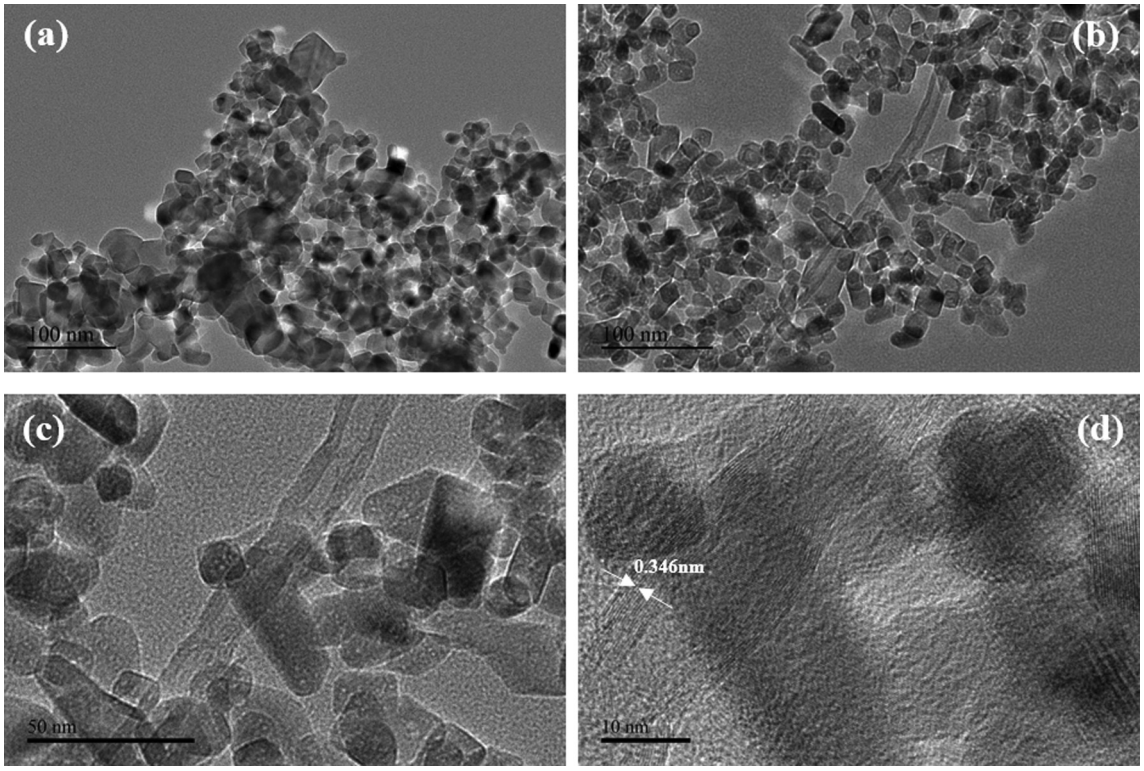

Fig. 2. TEM images of (a) pure TiO_2 particles (b–d) MWCNT-TiO_2 nanocomposite at various resolutions.

nanocomposite thin films is carried out and presented in Fig. 4, where the presence of peaks pertaining to the crystallographic planes of TiO_2 and MWCNT is quite evident. Particularly the relative intensity of (1 0 1) peak of TiO_2 increases with MWCNT concentration and this is because the diffraction intensity of (0 0 2) peak of MWCNT overlaps with that of (1 0 1) peak of TiO_2 which confirms their composite formation.

3.4. Raman analysis of nMWCNT-TiO_2 photo-anode

The Raman analysis is carried out using surface enhanced Raman spectroscopy to confirm the formation of composite in the fabricated thin films. Fig. 5a shows the Raman spectrum of all the synthesized composite photoanodes, where we can see the presence of the peaks due to different Raman modes of vibration of TiO_2 in the energy range of 100–800 cm^{-1} along with D and G bands of MWCNT in the energy of 1000–1600 cm^{-1}, which confirm the presence of both materials. The peak intensity of D and G bands increases as the amount of MWCNT increase. The magnified MWCNT peaks are provided in Fig. 5b and c, which clearly show the presence of MWCNT and their different compositions.

3.5. Optical absorption spectroscopy

The absorbance spectrum for N3 dye in ethanol in Fig. 6, (also in Fig. S1) shows two absorbance peaks in the visible spectral regions centered at 419 nm and 547 nm and one absorbance peak in the UV region centered at 322 nm. The visible region absorbance peaks, originate from the characteristic low energy metal to ligand charge transfer (MLCT), involving the excitation of electrons from 4d orbital of Ru to the unoccupied π^* molecular orbitals and also the absorbance peak in the ultra-violet (UV) region is due to ligand centered π–π^* excitation. When TiO_2 is added to N3, an electronic coupling between the N3 dye molecule and TiO_2 is established and this coupling reorganizes the energy structure in the intermolecular MLCT states. The titanium dioxide (TiO_2) effect of on the dynamics of the adsorbed N3 dye on its surface, is primarily due to both mode-specific vibrational and electronic de-phasing, where the latter process is more dominant. The restructuring of the intermolecular MLCT states, brought about by the presence of TiO_2, accompanied by efficient photo-induced charge transfer enhances the visible light absorbance on TiO_2-N3 dye as seen in Fig. 6. This visible light absorbance is further enhanced with the addition of MWCNT with the maximum visible light absorbance with 0.06% MWCNT in *n*-MWCNT-TiO_2 in the presence of N3 dye, as it is quite obvious from Fig. 6 and this further enhancement of visible light absorbance could be due to the photosensitizing property of MWCNT (Woan et al., 2009). However, with higher MWCNT content, the light transmission is restricted and also the agglomeration sets in, leading to reduced absorbance. In addition to the enhancement of overall absorbance in the visible spectral region, there is a slight red shift in the absorbance spectrum *n*-MWCNT-TiO_2, originating from the creation of defect states from the oxygen vacancy and/or structural defects in the MWCNT-TiO_2 composite, resulting from the formation of Ti—O—C bonds in the TiO_2 lattice. The observed red shift in the absorbance spectrum is attributed to the lowering of π^* energy level due to the bonding between carboxylic group in N3 dye and Ti^{4+} ion.

3.6. Photovoltaic performance of dye-sensitized solar cells

3.6.1. The current-voltage (J-V) characteristics of fabricated DSSC

The performance of the fabricated DSSC, having *n*-MWCNT-TiO_2 photosensitized by N3 dye as a photo-anode, and MWCNT as a counter electrode was evaluated by typical I-V characteristic study under standard test conditions (ambient temperature of 25 °C and 1 sun illumination, equivalent to 1000 W/cm^2 at air mass AM 1.5G) and the J-V curves are depicted in Fig. 7 for six different DSSC configurations. The key DSSC performance indicators like open circuit voltage V_{oc} (mV), short circuit current density J_{sc} (mA/cm^2), fill factor FF (%), and overall photovoltaic efficiency η (%) of all the configurations of DSSC, deduced from the I-V characteristics are listed in Table 2. In Fig. 7 the

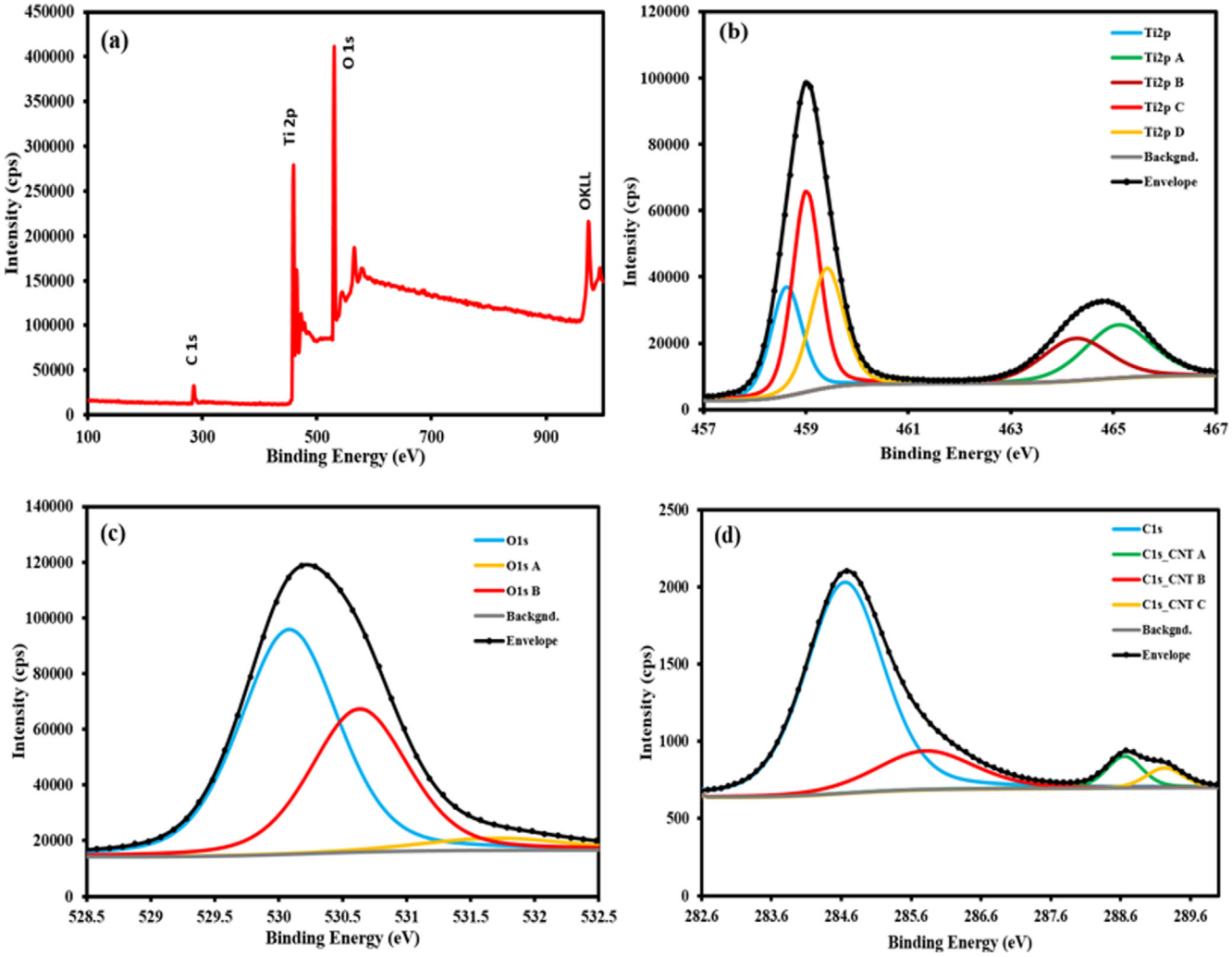

Fig. 3. XPS spectra of 0.06%-MWCNT-TiO_2 thin film: (a) Survey spectra (b) deconvolution of Ti 2p peak (c) deconvolution of O 1s peak and (d) deconvolution of C 1s spectra.

Table 1
Assignments of component peaks of deconvoluted Ti 2p, O 1s and C 1s.

Name	Peak BE	FWHM (eV)	Area (P) CPS.eV	Atomic %	Assignment
Ti2p	458.62	0.73	28949.39	17.59	TiO_2 ($2p_{3/2}$)
Ti2p A	465.1	1.56	29808.45	18.14	TiO_2 ($2p_{1/2}$)
Ti2p B	464.26	1.56	24162.46	14.7	TiO_2 ($2p_{1/2}$)
Ti2p C	459.01	0.64	47158.38	28.66	TiO_2 ($2p_{3/2}$)
Ti2p D	459.41	0.79	34405.05	20.91	TiO_2 ($2p_{3/2}$)
O1s	530.08	0.91	87351.31	58.49	SnO_2
O1s A	531.7	1.34	6823.62	4.57	Carbonates
O1s B	530.63	0.9	55159.78	36.94	TiO_2
C1s	284.65	1.32	2146.54	74.16	C—C
C1s_CNT A	288.65	0.6	147.66	5.1	C=O
C1s_CNT B	285.81	1.67	499.74	17.27	C—O
C1s_CNT C	289.23	0.64	100.59	3.48	O—C=O

photovoltaic output indicators of our proposed [*n*-MWCNT-TiO_2/N3/MWCNT] DSSC configuration with four different *n*-MWCNT-TiO_2 mass ratios (n = 0.03%, 0.06%, 0.09% and 0.12%) in photo anode are shown along with the standard [TiO_2/N719/Pt] and [TiO_2/N3/MWCNT] DSSC configurations for bench marking.

Table 2 indicates a systematic enhancement of short circuit current density J_{sc} for all the MWCNT based DSSCs and this is due to the improved electron transport property brought about by the presence of MWCNT. In the case of both [0.09%-MWCNT-TiO_2/N3/MWCNT] and [0.12%-MWCNT-TiO_2/N3/MWCNT] configurations, all the photovoltaic performance indicators are less than that of four other configurations presented in Fig. 7. This reduced photovoltaic performance in the above two configurations is due to the reduced visible light absorbance due to the agglomeration of MWCNT in the higher concentrations of MWCNT in photo anode, and also could be due to the formation of undesired trap states that facilitates the rapid photo induced charge recombination. Also, the higher recombination resistance (R_2) as explained in electrochemical impedance spectroscopy analysis of these fabricated DSSC provided in next section and the more intense visible light absorbance in [0.06%-MWCNT-TiO_2/N3/MWCNT] configuration should yield a higher short circuit current density J_{sc} for [0.06%-MWCNT-TiO_2/N3/MWCNT] configuration than that for [TiO_2/N719/Pt] configuration. But J_{sc} for [0.06%-MWCNT-TiO_2/N3/MWCNT] configuration listed in Table 2 is less than that of [TiO_2/N719/Pt] configuration and this discrepancy is due to the fact that the MWCNT presence in photoanode reduced the transparency and hence the number of electrons generated could be slightly lower in MWCNT-TiO_2 photo anodes than in [TiO_2/N719/Pt]. On the other hand, the fill factors and the efficiencies of [0.03%-MWCNT-TiO_2/N3/MWCNT] and [0.06%-MWCNT-TiO_2/N3/MWCNT] configurations are higher than that of [TiO_2/N3/MWCNT] and [TiO_2/N719/Pt] DSSC configurations, with the highest efficiency of 7.15% in the case of and [0.06%-MWCNT-TiO_2/N3/MWCNT]. This performance enhancement could be due to (i) the presence of optimum level of MWCNT in TiO_2, that serve as bridge

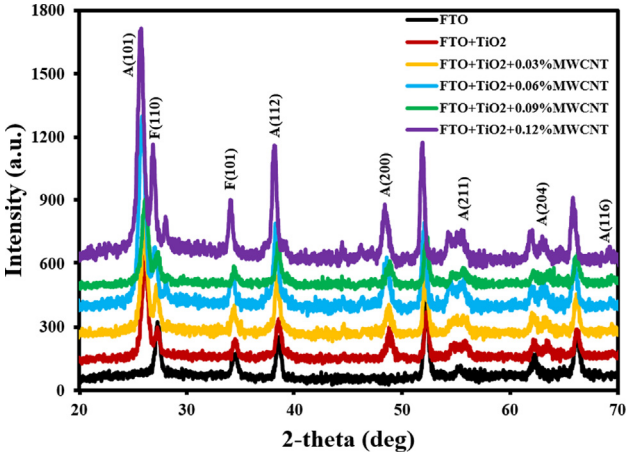

Fig. 4. XRD analysis of nMWCNT-TiO_2 nanocomposite thin films.

for the better transport of electrons without being trapped in the grain boundaries, thereby providing a conducting network for the transfer of photoelectron to the outer circuit of DSSC (Du et al., 2013; Batmunkh et al., 2015) (ii) the observed enhancement of visible light absorbance originating from the trap states formed due to the Ti—O—C bonds in the TiO_2 lattice, resulted in the generation of more photocurrents and (iii) the better catalytic performance at the counter electrode side, resulted in the enhancement of charges available for the efficient reduction of electrolyte (Nam et al., 2010). It is quite clear from this study that there is a 13% increase of efficiency in [0.06%-MWCNT-TiO_2/N3/MWCNT] DSSC configuration, compared to that of conventional DSSC configuration [TiO_2/N719/Pt].

3.6.2. Incident photon-to-electron conversion efficiency (IPCE)

The IPCE spectrum is the measure of external quantum efficiency (EQE) of a solar cell over a specific wavelength range, which gives the knowledge of efficient workability of the solar cell in a particular wavelength region. IPCE or EQE is basically the ratio of the number of electrons generated per second and the total number of photons falling on the solar cell from outside and due to many underlying wavelength dependent factors, EQE is a strong function of wavelength. Fig. 8 shows IPCE spectra of all the six variants of DSSCs fabricated in this work, and it is clear from the figure that although the pattern of spectral response of EQE is same for all the six DSSCs, the value of EQE remains the highest for 0.06%MWCNT-TiO_2 mass ratio for photoanode i.e. [*0.06% MWCNT*-TiO_2/N3/MWCNT] DSSC configuration. Also, we can notice that the EQE of all four variants of [*n*MWCNT-TiO_2/N3/MWCNT] DSSC are consistent. The IPCE (λ) depends highly on the wavelength dependent light harvesting efficiency of a solar cell (LHE (λ)), the yield of injecting photo-generated electrons to the conduction band of the semiconductor (φ_{inj}) and also the collection efficiency of the photo-generated electrons (η_{cc}), as described in Eq. (1) (Grätzel, 2005).

$$IPCE(\lambda) = LHE(\lambda)^{*}\varphi_{inj}{}^{*}\eta_{cc} \quad (1)$$

On the other hand, LHE (λ) depends on the dye adsorption on the surface of semiconductor, the light absorbance characteristics of the dye, and the light scattering at the photo-anode. The resemblance of IPCE spectrum in Fig. 8 to the absorbance spectrum of N3 dye in Fig. S1 and the observation of an optimum MWCNT content in [*n*MWCNT-TiO_2/N3/MWCNT] in Figs. 7 and 8 indicate these dependences of LHE (λ). Also, the presence of MWCNT in *n*MWCNT-TiO_2 nanocomposite promotes the injection of electron generated due to the photo-excited dye to the conduction band of MWCNT-TiO_2 nanocomposite semiconductor, resulting in the increase of φ_{inj} and makes MWCNT-TiO_2 more efficient by positively contributing to IPCE (λ) (Yang et al., 2016). The third parameter (η_{coll}) in Eq. (1) is associated with the charge recombination and charge transport properties of the semiconducting

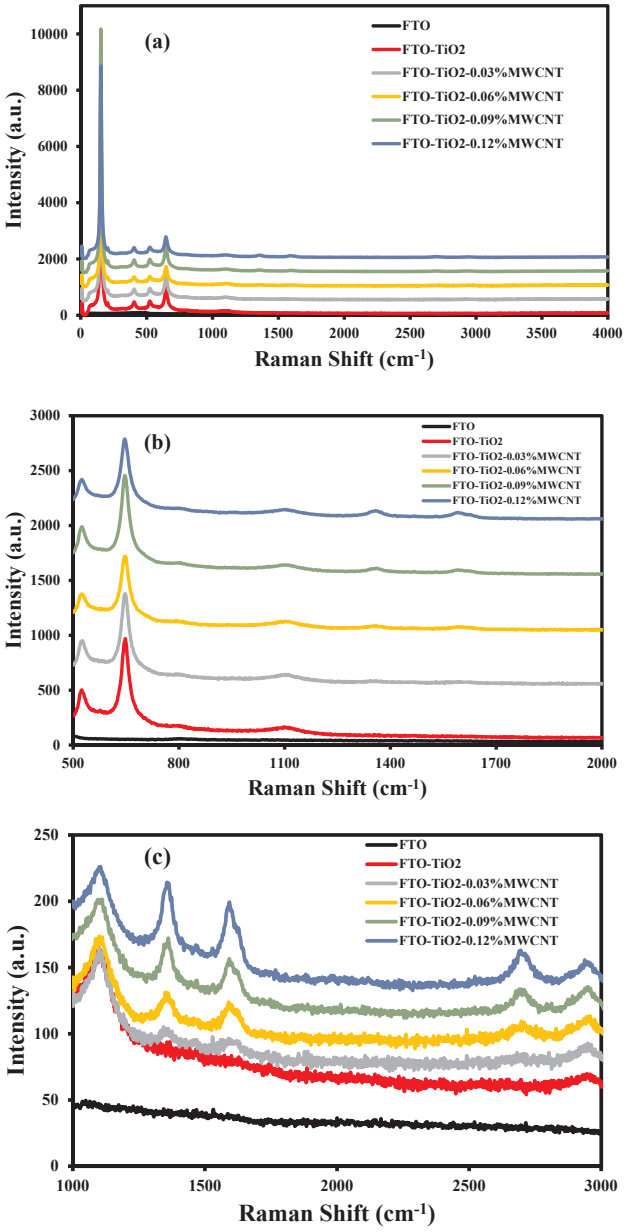

Fig. 5. Raman analysis of *n*MWCNT-TiO_2 thin films for (a) complete Raman spectra (b) Spectra from 500 cm^{-1} to 2000 cm^{-1} to focus on MWCNT peaks (c) Magnified MWCNT peaks in the range 1000 cm^{-1} to 3000 cm^{-1}.

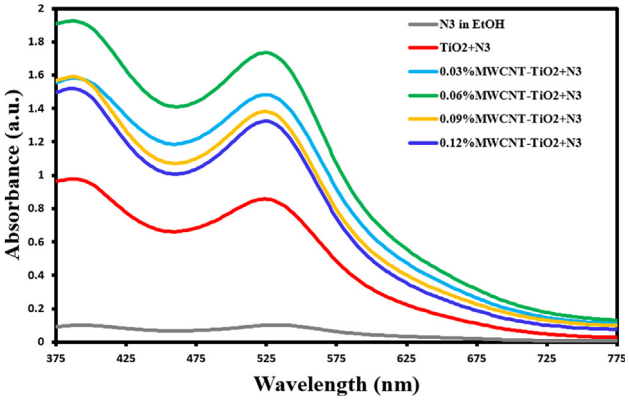

Fig. 6. UV–Vis spectra of N3 dye in EtOH, TiO_2/N3 and *n*-MWCNT-TiO_2/N3 films.

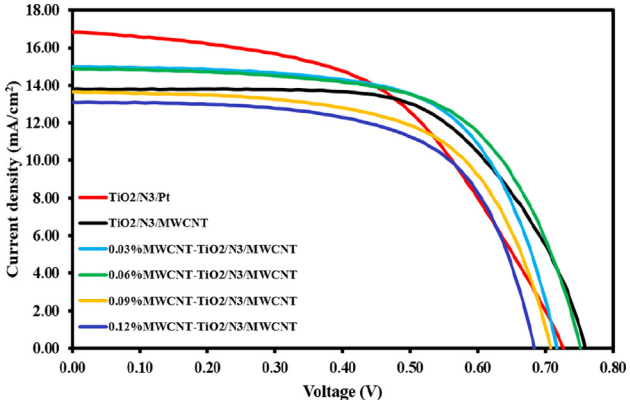

Fig. 7. J-V characteristics of fabricated DSSCs.

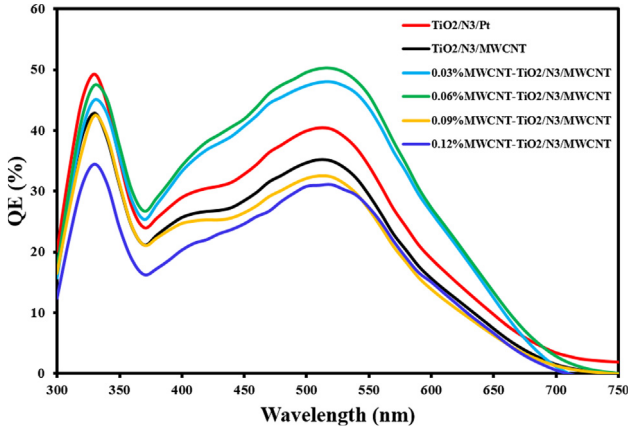

Fig. 8. IPCE spectra of fabricated DSSCs.

anode, which can be explained by electrochemical analysis. The electrochemical analysis shows that the MWCNT modified anodes DSSCs are better than unmodified anodes DSSCs and the resistance to the recombination of charges (R_2) is higher for modified photoanodes DSSCs compared to unmodified photoanodes DSSCs which is in good agreement with IPCE spectra.

3.6.3. Electrochemical impendence spectroscopy (EIS) analysis of fabricated DSSCs

In order to elucidate the electrochemical charge transfer and transport behavior in different pairs of charged surface layers and the media in DSSC during its operation, we carried out the EIS analysis at the open circuit voltage, in the 0.1 Hz – 10^5 Hz frequency range. The EIS results of all the six variants of DSSC are presented as Nyquist plots in Fig. 9. Further, the proposed equivalent circuit is provided in the inset of Fig. 9 and the numerical values of the fitted resistance and capacitance are listed in Table 3. Nyquist plot (in complex plane) is basically the wide range of frequency response of the imaginary and components of the cell impedance of the equivalent parallel RC circuits at different interfaces of DSSC. The smaller semicircles at the high frequency region (left) of the Nyquist plots in Fig. 9 arise due to the interface of MWCNT counter electrode and electrolyte, where R_1 is the charge transfer resistance and double layer C_1 represents capacitance due to the charge formation in back electrode layer and the electrolyte constitute RC network in the interface. The large semicircles at the mid frequency range are due to MWCNT-TiO_2/dye and electrolyte interface where R_2, the electron recombination (back reaction or dark current) resistance and C_2, the capacitance between the MWCNT-TiO_2 layer and the electrolyte constitute RC network in the interface. The third semicircles which is expected to appear at small frequency is due to characteristics of diffusion of the I^-/I^{3-} redox electrolytes are obscured due to much higher resistance of R_2 than that of Z_w (Warburg impedance). The Z_w is the impendence that is resistance encountered by the charge carriers when they diffused through the electrolyte. In addition to these, there is sheet resistance R_s that is in series with the RC parallel circuit, which is more or less similar for all the fabricated DSSCs. Except [TiO_2/N719/Pt] configuration, in all the other 5 variants of DSSCs, we use same MWCNT as the counter electrode, R_1 values are almost same with

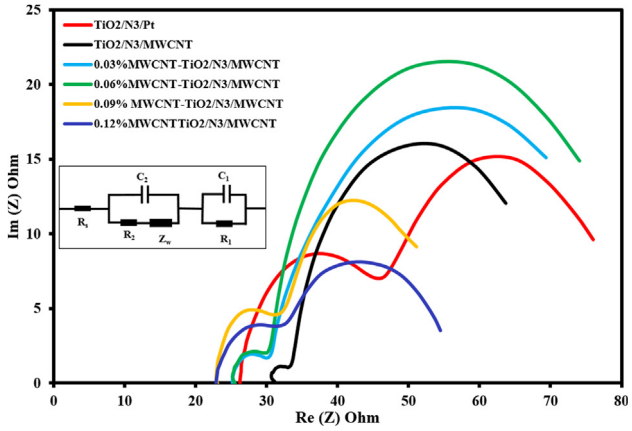

Fig. 9. EIS spectra of fabricated DSSCs with equivalent circuit of DSSC (inset).

Table 3
Equivalent circuit parameters of fabricated DSSCs.

Cell structure	R_1 (Ω)	R_2 (Ω)	C_1 (μF)	C_2 (mF)
TiO_2/N3/MWCNT	15.31	39.37	5.52	0.16
0.03%MWCNT-TiO_2/N3/MWCNT	8.95	41.54	20.57	0.26
0.06%MWCNT-TiO_2/N3/MWCNT	7.22	55.09	38.6	0.29
0.09%MWCNT-TiO_2/N3/MWCNT	19.74	27.28	19.7	0.23
0.12%MWCNT-TiO_2/N3/MWCNT	25.66	26.02	7.73	0.23
TiO_2/N3/Pt	23.45	36.67	5.28	0.25

slight variations. On the other hand, in the photo anode interface, the value of R_2 should vary according to the amount of MWCNT present in the photo anode material. The increased level of MWCNT photo anode facilitates the easy transport of the electrons within the semiconductor and also helps to reduce the recombination. It is quite clear from Fig. 9 and Table 3 that the recombination resistance R_2 corresponding to the configuration [0.06%-MWCNT-TiO_2/N3/MWCNT] based DSSC is the highest among the all six different fabricated configurations. This

Table 2
Photovoltaic properties of DSSCs.

Cell structure	J_{sc} (mA/cm^2)	V_{oc} (mV)	FF (%)	η (%)
TiO_2/N3/MWCNT	13.8 ± 0.1	759 ± 1	63 ± 1	6.65 ± 0.11
0.03%MWCNT-TiO_2/N3/MWCNT	14.9 ± 0.2	717 ± 2	64 ± 1	6.94 ± 0.11
0.06%MWCNT-TiO_2/N3/MWCNT	15.4 ± 0.1	752 ± 1	62 ± 1	7.15 ± 0.20
0.09%MWCNT-TiO_2/N3/MWCNT	13.6 ± 0.1	707 ± 1	62 ± 1	6.03 ± 0.08
0.12%MWCNT-TiO_2/N3/MWCNT	13.1 ± 0.2	683 ± 2	63 ± 1	5.69 ± 0.14
TiO_2/N3/Pt	16.8 ± 0.2	726 ± 2	52 ± 2	6.33 ± 0.35

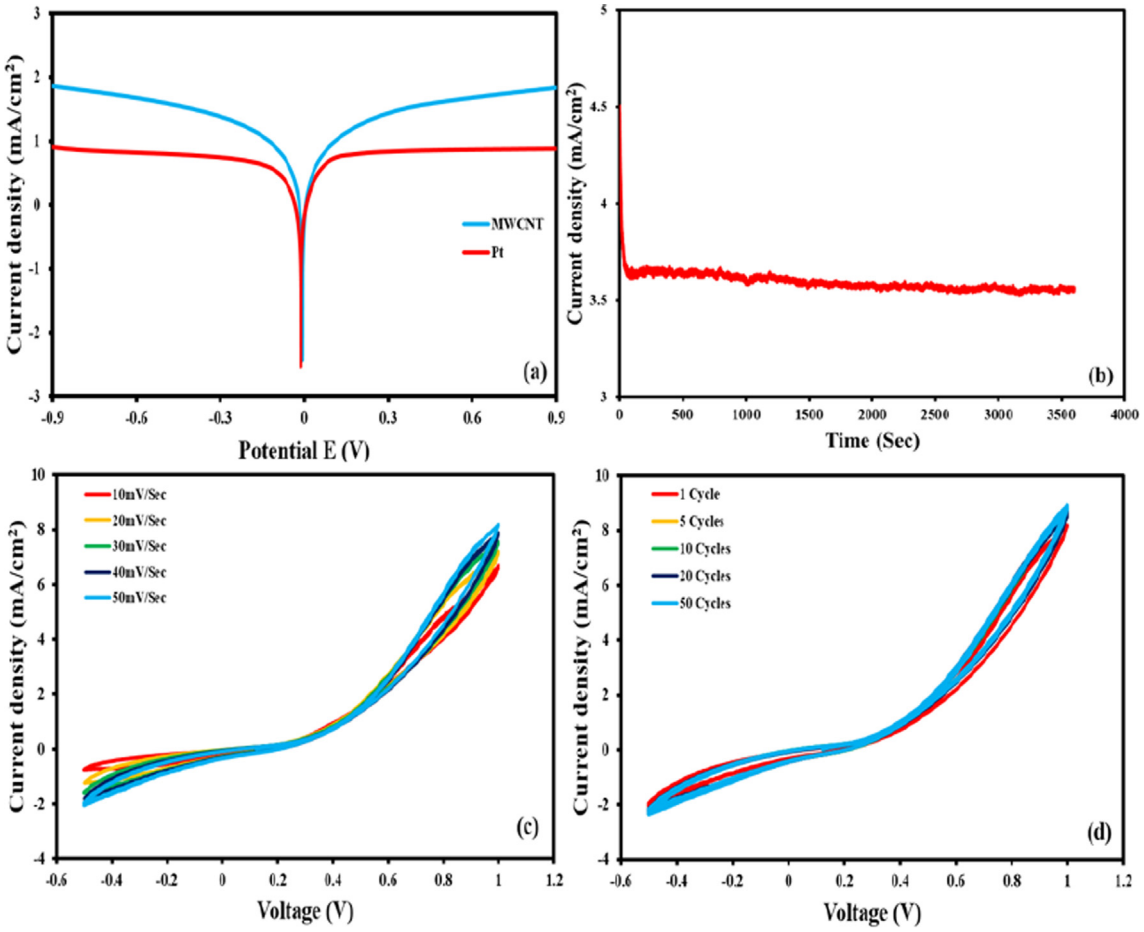

Fig. 10. (a) Tafel curves of symmetrical cells (dummy cells) fabricated with MWCNT and Pt. (b) Stability test of MWCNT as a catalyst for counter electrodes with 7.5 mM Iodolyte Z-50 as electrolyte, Pt as auxiliary electrode and Ag/AgCl as reference electrode, (c) Cyclic voltamograms for different scan rates, (d) CV curves at different number of cycles at the scan rate of 50 mV sec^{-1}.

largest R_2 in [0.06%-MWCNT-TiO_2/N3/MWCNT] configuration offers high resistance for the charge recombination (also called dark current) between the photosensitized electron in MWCNT-TiO_2 semiconducting surface and the electrolytic cationic layer surrounding MWCNT-TiO_2 directly from the conduction band of the photoanode (MWCNT-TiO_2) or through some trap states below (Mehmood et al., 2016b).

3.6.4. Catalytic activity of MWCNT

Besides the optical, electron transport and material characteristics of photo anode, the catalytic nature of the counter electrode (cathode), composition and configuration of DSSC, the nature of redox electrolytes and the sensitizing dye are the crucial factors that influence the performance of DSSC. Another improvisation introduced in the DSSC is the use of MWCNT as the catalytic material to replace the expensive platinum electrode. Although the [MWCNT-TiO_2/N3/MWCNT] DSSC is found to be more promising than the conventional [TiO_2/N3/Pt] configuration, it is quite interesting to single out the contribution of MWCNT counter electrode in the overall photovoltaic performance enhancement. In DSSC counter electrode functions as catalyst in the chemical process of efficiently reducing the redox mediator so that the dye molecules are rapidly regenerated. The rapid reduction of redox mediator and the regeneration of dye can also effectively inhibit the charge recombination at the conduction band of TiO_2 and electrolytic cations interface and also recombination of conduction electrons with the oxidized dye molecule. As the exchange current for the reduction of oxidized species in DSSC is proportional to the catalytic performance of the counter electrode material, we carried out Tafel analysis to estimate and compare the exchange current produced by the catalytic activity of Pt and MWCNT in the DSSC. We fabricated dummy cells for both MWCNT and Pt materials with Iodolyte I^-/I_3^- as electrolyte. Tafel plot is bases on the Tafel equation, in which the log *J;* logarithmic current density is plotted against the V; excess potential, and the exchange current can be deduced by taking the antilog of the y intercept (at V = 0) of the tangent of the curve. Fig. 10a shows the Tafel curves of dummy cells (also called symmetrical cells) fabricated with Pt and MWCNT, from which it is clear that the exchange current J_0 for MWCNT catalyst is considerably higher than that for Pt and hence it is quite obvious that the MWCNT as a counter electrode is found to be better than that of Pt in terms of catalytic activity in this DSSC configuration. The resistance R_1, at the electrolyte I^-/I_3^-/counter electrode interface called charge transfer has an inverse relation with exchange current density J_0 as shown in Eq. (2)

$$J_0 = \frac{RT}{nFR_1} \tag{2}$$

where F, R, T and n are Faraday's constant, the gas constant, temperature, and the number of electrons involved in the reduction reaction respectively. Hence according to Eq. (2), the increased J_0 for MWCNT is quite anticipated as the R_1 of the MWCNT as counter electrode estimated from the EIS study is found to be much less than that of Pt counter electrode (Table 3). Another important electrochemical parameter that can be deduced from Tafel plot is the limiting current (J_{lim}), which is the saturated level of current in the Tafel plot and from the Tafel plot in Fig. 10a, the limiting current for MWCNT catalyst is also found to be higher than that for Pt. The limiting current density (J_{lim}), is related to the diffusion coefficient (D) of the I^-/I_3^- redox

mediator as depicted in Eq. (3).

$$D = \frac{l}{2nFC} J_{lim} \quad (3)$$

where F is Faraday's constant, C is electrolyte concentration, l is the spacer thickness and n is the number of exchange electrons involved in the reduction reaction. Hence the improved exchange current and limiting current (improved diffusion coefficient) testify the role of MWCNT counter electrode to partially enhance the efficiency of [n-MWCNT-TiO_2/N3/MWCNT] DSSC.

3.6.5. Stability of MWCNT

Another desired feature of the counter electrode is that it should be chemically and electrochemically stable in the electrolytic environment. In this work chronoamperometry and cyclic voltammetry (CV) were carried out to study the chemical and electrochemical stability of MWCNTs as the CE. Fig. 10b is the results of chronoamperometric analysis, where the current density is found to be quite stable for the duration of 3600 s, when 600 mV potential was applied. Also cyclic voltammetry (CV) study was also carried out and the hysteresis loops formed due to the oxidation process (forward ramp of the voltage) and reduction process (reverse ramp of the voltage) remain quite similar in Fig. 10c and d, which are respectively for different number of cycles of forward/reverse voltage ramping (with the scan rate of 50 mV/sec) and for different voltage ramp rates. Therefore, it is quite evident from the chronoamperometric and cyclic voltammetric analyses that MWCNT counter electrode is electrochemically very stable.

4. Conclusion

In this work, MWCNT based DSSC was fabricated, where the synthesized MWCNT-TiO_2 nanocomposites with different levels of MWCNT were used as a photoanode in conjunction with MWCNT based, Pt free counter electrode. In photoanode, the presence of MWCNT in TiO_2 brought about many positive attributes like enhanced light absorbance in the visible spectral region, high electron recombination resistance and improved electron transportation. MWCNT in counter electrode showed better catalytic effect than Pt in the reduction reaction of the oxidized iodine/triiodine redox mediator in DSSC. All these improved features resulted in the enhancement of photovoltaic efficiency in the [n-MWCNT-TiO_2/N3/MWCNT] DSSCs, and among the four different compositions of MWCNT-TiO_2 nanocomposites used as a photoanode, the one with 0.06%-MWCNT-TiO_2, i.e. [0.06%-MWCNT-TiO_2/N3/MWCNT] DSSC configuration showed the highest photovoltaic efficiency of 7.15%, which accounts for an enhancement of 13% photovoltaic efficiency compared to the conventional [TiO_2/N3/Pt] DSSC configuration. This photovoltaic performance improvement and use of low cost MWCNT in the place of expensive platinum will make MWCNT based DSSCs efficient and cost effective for large scale applications. Morphological, optical, elemental and electrochemical studies of the material and DSSC were carried out and the improved photovoltaic efficiency of [n-MWCNT-TiO_2/N3/MWCNT] DSSC configuration is explained on the basis of these results.

Acknowledgement

We acknowledge the Deanship of Scientific Research, KFUPM, Saudi Arabia for supporting this work under the project# RG-161002 and also, we would like to thank Center of Research Excellence in Renewable Energy (CoRE-RE), Saudi Arabia for rendering their facilities for characterization studies. MAG acknowledges the funding support provided by the King Abdullah City for Atomic and Renewable Energy (K.A.CARE), Saudi Arabia under KACARE182-RFP-02 project.

Appendix A. Supplementary material

Supplementary data to this article can be found online at https://doi.org/10.1016/j.solener.2019.07.009.

References

Ahmed, U., Alizadeh, M., Rahim, N.A., Shahabuddin, S., Ahmed, M.S., Pandey, A.K., 2018. A comprehensive review on counter electrodes for dye sensitized solar cells: a special focus on Pt-TCO free counter electrodes. Sol. Energy 174, 1097–1125. https://doi.org/10.1016/j.solener.2018.10.010.

Arulraj, A., Ramesh, M., Subramanian, B., Senguttuvan, G., 2018. In-situ temperature and thickness control grown 2D-MoS2 via pulsed laser ablation for photovoltaic devices. Sol. Energy 174, 286–295. https://doi.org/10.1016/j.solener.2018.08.056.

Chandiran, A.K., Abdi-Jalebi, M., Nazeeruddin, M.K., Grätzel, M., 2014. Analysis of electron transfer properties of ZnO and TiO2 photoanodes for dye-sensitized solar cells. ACS Nano 8, 2261–2268. https://doi.org/10.1021/nn405535j.

Chen, M., Shao, L.-L., 2016. Review on the recent progress of carbon counter electrodes for dye-sensitized solar cells. Chem. Eng. J. 304, 629–645. https://doi.org/10.1016/j.cej.2016.07.001.

Chou, T.P., Zhang, Q., Russo, B., Fryxell, G.E., Cao, G., 2007. Titania particle size effect on the overall performance of dye-sensitized solar cells. J. Phys. Chem. C 111, 6296–6302. https://doi.org/10.1021/jp068939f.

Dale, M., 2013. A comparative analysis of energy costs of photovoltaic, solar thermal, and wind electricity generation technologies. Appl. Sci. 3, 325–337. https://doi.org/10.3390/app3020325.

Du, P., Song, L., Xiong, J., Li, N., Wang, L., Xi, Z., Wang, N., Gao, L., Zhu, H., 2013. Dye-sensitized solar cells based on anatase TiO2/multi-walled carbon nanotubes composite nanofibers photoanode. Electrochim. Acta 87, 651–656. https://doi.org/10.1016/j.electacta.2012.09.096.

Gondal, M.A., Ilyas, A.M., Baig, U., 2016a. Facile synthesis of silicon carbide-titanium dioxide semiconducting nanocomposite using pulsed laser ablation technique and its performance in photovoltaic dye sensitized solar cell and photocatalytic water purification. Appl. Surf. Sci. 378, 8–14. https://doi.org/10.1016/j.apsusc.2016.03.135.

Gondal, M.A., Ilyas, A.M., Baig, U., 2016b. Pulsed laser ablation in liquid synthesis of ZnO/TiO2 nanocomposite catalyst with enhanced photovoltaic and photocatalytic performance. Ceram. Int. 42, 13151–13160. https://doi.org/10.1016/j.ceramint.2016.05.104.

Gondal, M.A., Ilyas, A.M., Fasasi, T.A., Dastageer, M.A., Seddigi, Z.S., Qahtan, T.F., Faiz, M., Khattak, G.D., 2015. Synthesis of green TiO2/ZnO/CdS hybrid nano-catalyst for efficient light harvesting using an elegant pulsed laser ablation in liquids method. Appl. Surf. Sci. 357, 2217–2222. https://doi.org/10.1016/j.apsusc.2015.09.213.

Gracia, F., Holgado, J.P., González-Elipe, A.R., 2004. Photoefficiency and optical, microstructural, and structural properties of TiO2 thin films used as photoanodes. Langmuir 20, 1688–1697. https://doi.org/10.1021/la034998y.

Grätzel, M., 2009. Recent advances in sensitized mesoscopic solar cells. Acc. Chem. Res. 42, 1788–1798. https://doi.org/10.1021/ar900141y.

Grätzel, M., 2003. Dye-sensitized solar cells. J. Photochem. Photobiol. C Photochem. Rev. 4, 145–153. https://doi.org/10.1016/S1389-5567(03)00026-1.

Grätzel, Michael, 2005. Solar energy conversion by dye-sensitized photovoltaic cells. Inorg. Chem. 44 (20), 6841–6851. https://doi.org/10.1021/ic0508371. https://pubs.acs.org/doi/10.1021/ic0508371.

Gregg, B.A., Pichot, F., Ferrere, S., Fields, C.L., 2001. Interfacial recombination processes in dye-sensitized solar cells and methods to passivate the interfaces. J. Phys. Chem. B 105, 1422–1429. https://doi.org/10.1021/jp003000u.

Hagfeldt, A., Boschloo, G., Sun, L., Kloo, L., Pettersson, H., 2010. Dye-sensitized solar cells. Chem. Rev. 110, 6595–6663. https://doi.org/10.1021/cr900356p.

Hardin, B.E., Snaith, H.J., McGehee, M.D., 2012. The renaissance of dye-sensitized solar cells. Nat. Photon. 6, 162–169. https://doi.org/10.1038/nphoton.2012.22.

Ilyas, A.M., Gondal, M.A., Baig, U., Akhtar, S., Yamani, Z.H., 2016. Photovoltaic performance and photocatalytic activity of facile synthesized graphene decorated TiO2 monohybrid using nanosecond pulsed ablation in liquid technique. Sol. Energy 137, 246–255. https://doi.org/10.1016/j.solener.2016.08.019.

Iqbal, M.Z., Khan, S., 2018. Progress in the performance of dye sensitized solar cells by incorporating cost effective counter electrodes. Sol. Energy 160, 130–152. https://doi.org/10.1016/j.solener.2017.11.060.

Jacoby, M., 2016. The future of low-cost solar cells. Chem. Eng. News 94, 30–35.

Karthick, R., Arulraj, A., Ramesh, M., Selvaraj, M., 2018. Free-standing graphene/NiMoS paper as cathode for quasi-solid state dye-sensitized solar cells. J. Colloid Interface Sci. 530, 179–188. https://doi.org/10.1016/j.jcis.2018.06.082.

Lee, K.S., Lee, H.K., Wang, D.H., Park, N.-G., Lee, J.Y., Park, O.O., Park, J.H., 2010. Dye-sensitized solar cells with Pt- and TCO-free counter electrodes. Chem. Commun. 46, 4505. https://doi.org/10.1039/c0cc00432d.

Li, B., Wang, L., Kang, B., Wang, P., Qiu, Y., 2006. Review of recent progress in solid-state dye-sensitized solar cells. Sol. Energy Mater. Sol. Cells 90, 549–573. https://doi.org/10.1016/j.solmat.2005.04.039.

Mehmood, U., 2017. Efficient and economical dye-sensitized solar cells based on graphene/TiO2 nanocomposite as a photoanode and graphene as a Pt-free catalyst for counter electrode. Org. Electron. 42, 187–193. https://doi.org/10.1016/j.orgel.2016.12.039.

Mehmood, U., Aslam, H.Z., Al-Sulaiman, F.A., Al-Ahmed, A., Ahmed, S., Malik, M.I., Younas, M., 2016a. Electrochemical impedance spectroscopy and photovoltaic analyses of dye-sensitized solar cells based on carbon/TiO2 composite counter electrode. J. Electrochem. Soc. 163, H339–H342. https://doi.org/10.1149/2.0111606jes.

Mehmood, U., Hussein, I.A., Harrabi, K., Tabet, N., Berdiyorov, G.R., 2016b. Enhanced photovoltaic performance with co-sensitization of a ruthenium(II) sensitizer and an organic dye in dye-sensitized solar cells. RSC Adv. 6, 7897–7901. https://doi.org/10.1039/C5RA26577K.

Mehmood, U., Rahman, S., Harrabi, K., Hussein, I.A., Reddy, B.V.S., 2014. Recent advances in dye sensitized solar cells 0–13. doi: 10.1155/2014/974782.

Mehmood, U., Ul Haq Khan, A., Ali Qaiser, A., Bashir, S., Younas, M., 2018. Nanocomposites of carbon allotropes with TiO2 as effective photoanodes for efficient dye-sensitized solar cells. Mater. Lett. 228, 125–128. https://doi.org/10.1016/j.matlet.2018.05.127.

Batmunkh, Munkhbayar, Biggs, Mark J., Shapter, Joseph G., 2015. Carbonaceous dye--sensitized solar cell photoelectrodes. Adv. Sci. 2, 16. https://doi.org/10.1002/advs.201400025.

Nakade, S., Saito, Y., Kubo, W., Kitamura, T., Wada, Y., Yanagida, S., 2003. Influence of TiO2 nanoparticle size on electron diffusion and recombination in dye-sensitized TiO2 solar cells. J. Phys. Chem. B 107, 8607–8611. https://doi.org/10.1021/jp034773w.

Nam, J.G., Park, Y.J., Kim, B.S., Lee, J.S., 2010. Enhancement of the efficiency of dye-sensitized solar cell by utilizing carbon nanotube counter electrode. Scr. Mater. 62, 148–150. https://doi.org/10.1016/j.scriptamat.2009.10.008.

Nugent, J.M., Santhanam, K.S.V., Rubio, A., Ajayan, P.M., 2001. Fast electron transfer kinetics on multiwalled carbon nanotube microbundle electrodes. Nano Lett. 1, 87–91. https://doi.org/10.1021/nl005521z.

O'Regan, B., Grätzel, M., 1991. A low-cost, high-efficiency solar cell based on dye-sensitized colloidal TiO2 films. Nature 353, 737–740. https://doi.org/10.1038/353737a0.

Qiu, B., Zhou, Y., Ma, Y., Yang, X., Sheng, W., Xing, M., Zhang, J., 2015. Facile synthesis of the Ti3+ self-doped TiO2-graphene nanosheet composites with enhanced photocatalysis. Sci. Rep. 5, 8591. https://doi.org/10.1038/srep08591.

Roy-Mayhew, J.D., Aksay, I.A., 2014. Graphene materials and their use in dye-sensitized solar cells. Chem. Rev. 114, 6323–6348. https://doi.org/10.1021/cr400412a.

Ruhle, K., Juhl, M.K., Abbott, M.D., Kasemann, M., 2015. Evaluating crystalline silicon solar cells at low light intensities using intensity-dependent analysis of I-V parameters. IEEE J. Photovolt. 5, 926–931. https://doi.org/10.1109/JPHOTOV.2015.2395145.

Iijima, S., 1991. Helical microtubules of graphitic carbon. Nature 354, 56–58.

Sanjinés, R., Tang, H., Berger, H., Gozzo, F., Margaritondo, G., Lévy, F., 1994. Electronic structure of anatase TiO2 oxide. J. Appl. Phys. 75, 2945–2951. https://doi.org/10.1063/1.356190.

Shuttleworth, D., 1980. Preparation of metal-polymer dispersions by plasma techniques. An ESCA investigation. J. Phys. Chem. 84, 1629–1634. https://doi.org/10.1021/j100449a038.

Sleigh, C., Pijpers, A.P., Jaspers, A., Coussens, B., Meier, R.J., 1996. On the determination of atomic charge via ESCA including application to organometallics. J. Electron Spectros. Relat. Phenomena 77, 41–57. https://doi.org/10.1016/0368-2048(95)02392-5.

Tettey, K.E., Yee, M.Q., Lee, D., 2010. Photocatalytic and conductive MWCNT/TiO2 nanocomposite thin films. ACS Appl. Mater. Interfaces 2, 2646–2652. https://doi.org/10.1021/am1004656.

Woan, K., Pyrgiotakis, G., Sigmund, W., 2009. Photocatalytic carbon-nanotube-TiO2 composites. Adv. Mater. 21, 2233–2239. https://doi.org/10.1002/adma.200802738.

Wu, J., Lan, Z., Lin, J., Huang, M., Huang, Y., Fan, L., Luo, G., Lin, Y., Xie, Y., Wei, Y., 2017. Counter electrodes in dye-sensitized solar cells. Chem. Soc. Rev. 46, 5975–6023. https://doi.org/10.1039/C6CS00752J.

Ye, M., Wen, X., Wang, M., Iocozzia, J., Zhang, N., Lin, C., Lin, Z., 2015. Recent advances in dye-sensitized solar cells: from photoanodes, sensitizers and electrolytes to counter electrodes. Mater. Today 18, 155–162. https://doi.org/10.1016/j.mattod.2014.09.001.

Younas, M., Gondal, M.A., Dastageer, M.A., Baig, U., 2018a. Fabrication of cost effective and efficient dye sensitized solar cells with WO3-TiO2 nanocomposites as photoanode and MWCNT as Pt-free counter electrode. Ceram. Int. https://doi.org/10.1016/j.ceramint.2018.09.269.

Younas, M., Gondal, M.A., Mehmood, U., Harrabi, K., Yamani, Z.H., Al-Sulaiman, F.A., 2018b. Performance enhancement of dye-sensitized solar cells via cosensitization of ruthenizer Z907 and organic sensitizer SQ2. Int. J. Energy Res. https://doi.org/10.1002/er.4154.

Zulkifili, A.N.B., Kento, T., Daiki, M., Fujiki, A., 2015. The basic research on the dye-sensitized solar cells (DSSC). J. Clean Energy Technol. 3, 382–387. https://doi.org/10.7763/JOCET.2015.V3.228.